Influence of Particle Geometry Assessed via Image Processing on Broken Sandstone Strength

S. Balideh[1,*], T.G. Joseph[1] and M. Curley[1]

[1]*University of Alberta, Department of Civil & Environmental Engineering, School of Mining & Petroleum Engineering, 7-203 Donadeo Innovation Centre for Engineering, Edmonton, Alberta, Canada*

Abstract: Particle geometry has an impact on the behavior and strength of broken rock, where particle shape characteristics affect the ability of particles to rotate or slide relative to each other. Form, angularity and texture are three independent parameters that describe the geometry of such a particle. In this paper the geometry of crushed Berea sandstone was determined through image processing, where the results showed that form and angularity indices describe the geometry characteristics of broken Berea sandstone better than the other geometry indices. A correction coefficient that has previously been introduced to predict a sieve size distribution from image processing was shown to be a function of form index for the sandstone fragments. Triaxial compression tests were performed on the broken sandstone, showing that confining pressure and void ratio have an impact on broken rock strength. Increasing confining pressure was shown to enhance the strength of broken rock, while void ratio was shown to be inversely related to broken rock strength. Void ratio can also be affected by particle geometry. Increasing particles form index increases the void ratio where particles angularity index and void ratio are inversely related.

Keywords: Broken rock, Triaxial test, Shape, Geometry, Angularity, Form, Roughness, Friction, Void ratio.

1. INTRODUCTION

The behavior of broken rock plays a significant role in construction and mining projects. A good understanding of the behavior of broken rock helps us to make more informed decisions regarding geo-structures. Backfill design, waste dumps, rockfill engineering and slope stability indicate the significance of broken rock strength. The behavior of broken rock is influenced by material strength properties and geometric shape parameters. Interaction between discrete particles specifically impacts the behavior of broken rock, seen as a combination of the following interaction mechanisms: Sliding resistance between particles; resistance of particles to roll and particle breakage.

The frictional resistance of broken rock is influenced by two key considerations: The sliding of particles relative to each other and the resistance of particles to roll. Based on Amontons laws [1], the frictional resistance is independent of the size of the inter-particle contact area but is directly affected by the applied normal load. Marsal [2, 3] illustrated that for the broken rock, the average frictional resistance for a given composition of particles is proportional to the average contact force between them. The resulting normal stress between particle contact surfaces effectively induces a lateral confining pressure; which explains why broken rock strength under triaxial conditions is sensitive to confining pressure. In considering the resistance to roll, Marsal showed that the shape of particles and the number of contacts between adjacent particles significantly impacts the resistance to roll. It can be concluded from Marsal's research that the geometry of particles affects sliding, rolling, and to a lesser degree breakage and therefore the overall behavior of a broken rock.

Void ratio impacts bulk density of broken rock which is directly related to broken rock strength. Broken rock with low void ratio presents a higher density and strength. Mogami [4] calculated the internal friction angle for broken rock using a direct shear box and triaxial compression tests. He inferred that the internal friction angle is inversely related to void ratio. Triaxial test results also performed by Mogami showed the same inverse relationship between void ratio and broken rock strength. Fumagalli [5] carried out triaxial tests on broken rock to study the behavior of cohesionless material for rockfill dams. He demonstrated that broken rock void ratio has a significant impact on the effective modulus of broken rock, decreasing with void ratio increase.

Hobbs [6, 7] also investigated the behavior of broken rock using triaxial compression tests, showing that confining pressure has an impact on the peak strength; and resulting in a criterion to predict the strength of broken rock as a function of confining pressure. Hobbs further demonstrated an effective

*Address correspondence to this author at the University of Alberta, Department of Civil & Environmental Engineering, School of Mining & Petroleum Engineering, 7-203 Donadeo Innovation Centre for Engineering, 9211 - 116 Street NW, T6G 1H9, Edmonton, Alberta, Canada;
E-mail: balideh@ualberta.ca

E-ISSN: 2409-5710/18

Young's modulus for broken rock as a function of applied confining pressure. Hussaini [8-10] tested the behavior of crushed basalt and found that the relationship between major and minor principal stress is non-linear. Hussaini believed that confining pressure and grain size generated the largest impact on broken rock strength, such that particle size enhances the ultimate strength of broken rock. Joseph and Barron [11, 12] developed a post failure strength criterion for rock relative to the strength of the intact rock state. They showed that effective friction angle, intact rock properties, confining pressure and particle size all have a major impact on the strength of broken rock.

Previous studies on the behavior of broken rock indicate the influence of particle geometry on broken rock strength. Determining dimensions of a particle directly using simple equipment is not new, however, the nature of coarse particle shapes does not permit a geometric description of a coarse particle solely by measuring simple dimensions. Barrett [13], Masad [14-16], Little [17], Al-Rousan [18, 19] inferred that the geometry of particles can be explained through three independent characteristics to explain more fully the geometry of a particle: Form, angularity and texture.

Azevedo and Lemos [20], Zhou [21], Afshar [22], Chen and An [23] illustrated the impact of particle geometry and size distribution on the mechanical and physical properties of broken rock. Measuring particle dimensions is a first step to determine geometric characteristics. Figure **1** illustrates these parameters.

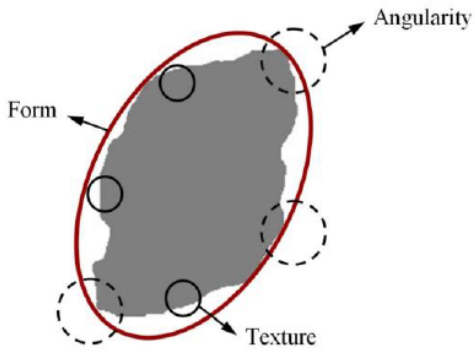

Figure 1: The concept of form, angularity and texture of a particle

Form expresses the overall shape of a particle, where particles may be similar to triangles, circles, quadrangles or other shapes. Angularity describes the variation in the apex angles of a particle. Texture expresses the surface inequality or roughness at such a scale that it does not impact the shape of the particle.

Form factor, expressed by Equation 1, has been used frequently to describe the overall shape of an aggregate particle as a dimensionless parameter. Masad [24], Wang [25], Arasan [26] used Equation 1 to evaluate form factor where circular particles have a form factor equal to one and elliptical particles less than one.

$$FormFactor = \frac{4A\pi}{P^2} \quad (1)$$

Where A is the surface area and P is the perimeter of an aggregate particle.

Little [17] and Masad [27] introduced form index as a dimensionless parameter that reflects the form of particles determined via Equation 2, where a reference of zero is adopted for spherical particles; and for elliptical particles is greater than zero.

$$FormIndex = \sum_{\theta=0}^{\theta=360-\Delta\theta} \frac{\left|R_{\theta+\Delta\theta} - R_{\theta}\right|}{R_{\theta}} \quad (2)$$

Where R_θ is the radius of a particle in a defined direction θ, and the radius of the particle is the length between the geometric center and the boundary of the particle at the defined angle θ. Figure **2** illustrates the radius of the particle at a direction θ.

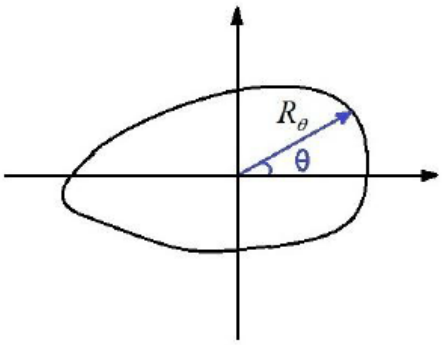

Figure 2: The concept of radius of the particle in a direction θ.

Roundness describes the form of particles as a dimensionless parameter that is the inverse of form factor; equal to one for circular particles and greater than one for elliptical particles, Equation 3.

$$Roundness = \frac{1}{FormFactor} \quad (3)$$

Masad [14] and Al-Rousan [18] introduced an angularity index to quantify the angularity of particles as a normalized difference between particle radius and

equivalent ellipsoid radius in a given direction. Equation 4 expresses angularity index as a dimensionless parameter equal to zero for a spherical particle.

$$AngularityIndex = \sum_{\theta=0}^{\theta=360-\Delta\theta} \frac{\left|R_\theta - R_{EE\theta}\right|}{R_{EE\theta}} \quad (4)$$

Where R_θ is the radius of a particle in a direction θ and $R_{EE\theta}$ is the radius of the equivalent ellipsoid in the same θ direction. The equivalent ellipsoid has the same area, as well as the same first and second-degree moment of the particle.

Masad [14], Kuo and Freeman [28] introduced Equation 5 to define an angularity parameter referenced as a dimensionless value of one for a spherical particle.

$$AngularityParameter = \left(\frac{P_{convex}}{P_{ellipse}}\right)^2 \quad (5)$$

Where P_{convex} is the perimeter of a bounding polygon surrounding the particle and $P_{ellipse}$ is a perimeter of the equivalent ellipsoid.

An intensity histogram method was developed by Masad [16] from the earlier work of Little [17] to describe the surface texture where the intensity of each image pixel of a particle surface is proportional to the roughness and inequality of a particle surface; implying that the mean and standard deviation of a particle surface intensity may represent the texture of a particle.

A texture parameter has been suggested to describe the surface texture of particles, such that Kuo and Freeman [28] and later Masad [16], developed Equation 6 to determine such a texture parameter a dimensionless and equal to one for a completely smooth particle and greater than one for a rough particle.

$$TextureParameter = \left(\frac{P}{P_{convex}}\right)^2 \quad (6)$$

Where P is the perimeter of the particle and P_{convex} is the perimeter of an encompassing bounding polygon.

More recently, image processing techniques have been used extensively to quantify particle geometry (Tutumluer [29], Fletcher [30], Swift [31], Wang [32], Koohmishi and Palassi [33]). Generally, an image is represented as a 2D signal where image parameters are proportional to the amplitude of the signal. In this paper, the photo of a particle was processed as an RGB image where each pixel contained data on the intensity of red, green and blue colors.

In the research conducted for this paper, specimens with different particle geometry were investigated using triaxial compression tests at low confining pressure. The triaxial compression test was identified as the best choice to examine the behavior of broken rock because it provides acceptable conditions for deformation of a specimen without imposing any preset failure plane on a specimen. For performing triaxial tests, soil triaxial cell employed because it is compatible with thin membranes to reduce the effect of the membrane on specimen deformation. Before performing triaxial compression test, particle geometry of specimen was determined using image processing techniques. Finally, the result of triaxial compression tests was analyzed to investigate the relationship between particle geometry and strength of broken rock.

2. A REVISED IMAGE PROCESSING TECHNIQUE

Here, a high-resolution particle photograph was used as input data for image processing. Poor lighting around particles produced shadows and consequently made particle boundary determination difficult. As such, a 'back-light' box was built to provide constant lighting conditions. The resolution of the photo was then established to recognize the boundary of a particle via image processing. Commercial cameras have sufficient resolution; however, a minimum of 100 pixels per diameter of a particle were established as a minimum for angularity analysis, [16]. Figure **3** shows the light box used here, and a photograph taken over the light box.

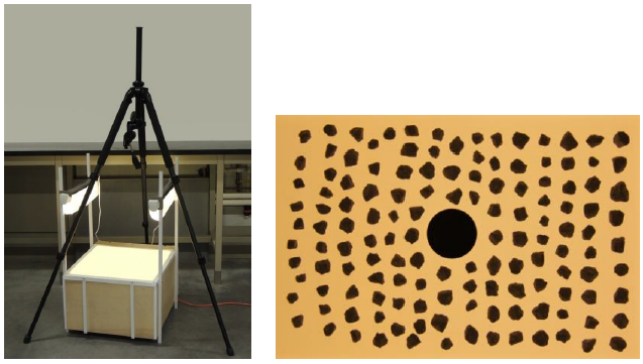

Figure 3: The light box and a photograph taken over the light box.

The RGB image was then converted to a binary photo, permitting the boundary of a particle to be

clearly established for processing. In the RGB image, each pixel consisted of three numbers to identify the color, (0 to 255, corresponding to the intensity of a color). For the pixels of a binary image there were only 0 or 1 values, white pixels having values of 1 and black pixels having values of 0. Recognizing the boundary pixels of a particle in a binary image was hence a much simpler process.

Unwanted very small particles such as dust often appear when taking particle photos, generating errors. The number of pixels per particle diameter was set as a criterion to auto-delete unwanted particles in processing. Determining the threshold number of pixels was found through trial and error to establish the pixel number to avoid a majority of unwanted small size particles. Figure **4** shows a binary image of the RGB Photo before and after deleting unwanted small particles.

Similarly, in binary images of RGB images, reflective surface generated “holes” may appear within a particle. The surface of particles is not smooth, and the color intensity varies proportionally; therefore, some pixels within a particle may have a white color in a converted binary image seen as holes inside the particle. All such holes were filled via the value of any pixel inside a particle that was 1 changed to 0. Figure **5** illustrates a binary image and filling of a hole inside a particle.

Pixels at the boundary of a particle were identified, using MATLAB to seek and identify the number and type of pixels in horizontal and vertical directions, corresponding to x and y Cartesian axes. Equations 1 through 6 were coded to determine shape parameters for each particle via boundary pixel relative locations.

3. EXAMPLE GEOMETRY CHARACTERISTICS OF BROKEN BEREA SANDSTONE

The particles of broken rock specimens were created from Berea sandstone passing a jaw crusher with a gape of 1cm, and then sieved to remove particles < 6 mm and > 12 mm. The homogenous Berea sandstone had a very fine grain structure with a density of 2300 kg/m^3. The image processing method and coded equations were used to determine the geometry characteristics of particles for each specimen prior to performing triaxial compression test. In Table **1** for each specimen, the average of the particles geometry characteristic was reported as geometry characteristic of the corresponding specimen.

Table **1** shows that the texture parameter (TP) had little variance but commensurate with the particle surface roughness. Form index (FI) and angularity

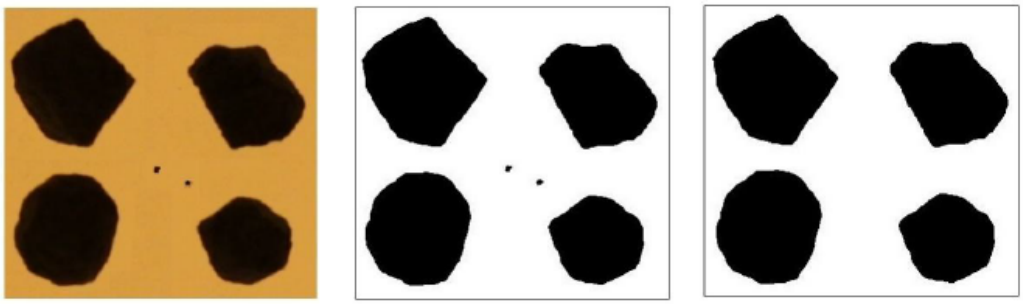

Figure 4: Removal of unwanted small particles.

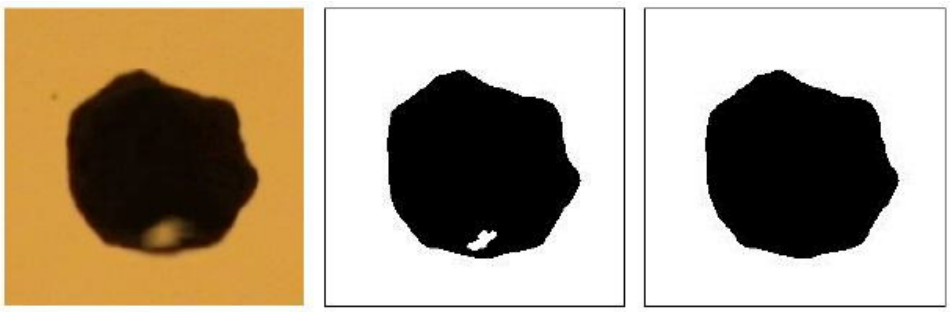

Figure 5: Filling resolution holes in particle images.

Table 1: The Particle Geometry of Specimens Determined by Image Processing Technique

Specimen No.	FI	FF	Roundness	AI	AP	TP
S 1	1.534	0.836	1.196	16.398	1.057	1.105
S 2	3.081	0.707	1.425	29.042	1.056	1.116
S 3	2.164	0.788	1.272	22.612	1.070	1.105
S 4	2.550	0.727	1.382	38.220	1.089	1.141
S 5	3.058	0.701	1.435	33.150	1.072	1.118
S 6	2.204	0.772	1.298	28.369	1.083	1.119
S 7	2.726	0.728	1.384	32.356	1.083	1.118
S 8	3.141	0.693	1.454	33.057	1.071	1.120
S 9	1.506	0.841	1.190	15.331	1.055	1.102
S 10	2.943	0.718	1.399	26.196	1.060	1.114
S 11	2.185	0.788	1.272	19.795	1.069	1.104
S 12	2.605	0.751	1.338	23.020	1.061	1.110
S 13	2.535	0.731	1.375	36.417	1.090	1.138
S 14	1.513	0.841	1.191	15.505	1.055	1.102
S 15	2.783	0.734	1.369	24.420	1.062	1.114
S 16	2.235	0.784	1.280	20.922	1.067	1.104
S 17	2.444	0.743	1.352	35.435	1.088	1.131
S 18	1.615	0.826	1.212	18.690	1.058	1.112
S 19	2.713	0.737	1.365	29.021	1.064	1.125
S 20	2.104	0.786	1.277	24.709	1.070	1.115
S 21	2.574	0.743	1.352	28.143	1.067	1.123
S 22	1.598	0.828	1.211	18.849	1.057	1.111
S 23	2.595	0.744	1.351	28.198	1.062	1.120
S 24	1.616	0.826	1.213	19.599	1.057	1.112
S 25	2.140	0.783	1.281	26.438	1.071	1.118
S 26	1.945	0.797	1.262	20.431	1.068	1.118
S 27	2.535	0.747	1.345	26.382	1.070	1.123

Table 2: Statistical Parameters of Particle Geometry of Specimens

	FI	FF	Roundness	AI	AP	TP
Minimum	1.506	0.693	1.190	15.331	1.055	1.102
Maximum	3.141	0.841	1.454	38.220	1.090	1.141
Average	2.320	0.767	1.314	25.582	1.068	1.116
Standard Deviation	0.513	0.045	0.080	6.501	0.011	0.010
Range	1.635	0.148	0.264	22.889	0.035	0.039
Variation %	22.112	5.867	6.088	25.412	1.030	0.896

index (AI) had a higher proportionate variability, and thus considered as a better indicator of varying particle geometric characteristic for the crushed Berea sandstone. Form factor (FF), roundness and angularity parameter (AP) also exhibited variation with particle shape, but to a marked lesser extent. Table **2** provides average, minimum, maximum, standard deviation, range and variation of shape parameters for all specimens.

Form index and angularity index impact the void ratio for broken rock. The geometry of particles

influences the void space between particles and consequently changes the void ratio. The void ratio of a specimen is the ratio of the void space between particles to the volume of particles. To determine the void ratio of a broken rock specimen, it is assumed that the particles are completely solid and the void space inside the intact rock was not taken in to account. The void ratio can be calculated by using Equation 7.

$$e = \frac{V_v}{V_s} \tag{7}$$

Where V_v is the volume of void spaces between particles and V_s is the volume of solids (particles).

The distribution of void spaces between solid particles has been investigated in applied mathematics as a packing problem, where Gray [34], Donev [35] and Delaney and Cleary [36] illustrated that the shape of particles impact packing density and void space between particles. Delaney and Cleary [36] used an ellipsoid analogy to define the shape of particles relative to void ratio. They illustrated that an increasing aspect ratio and decreasing shape parameter decreased packing density. If particles of broken rock are in full contact, packing density and void ratio are inversely related. In this paper the relationship between void ratio and the geometry of particles was investigated, where geometric shapes with a known aspect ratio and shape parameter were evaluated, and then the form index and angularity index of the shapes were calculated using MATLAB. Based on the results, convex particles exhibited form index proportional to void ratio, while angularity index and void ratio were inversely related. Figure **6** shows the relationship between form index and void ratio for varying angularity index.

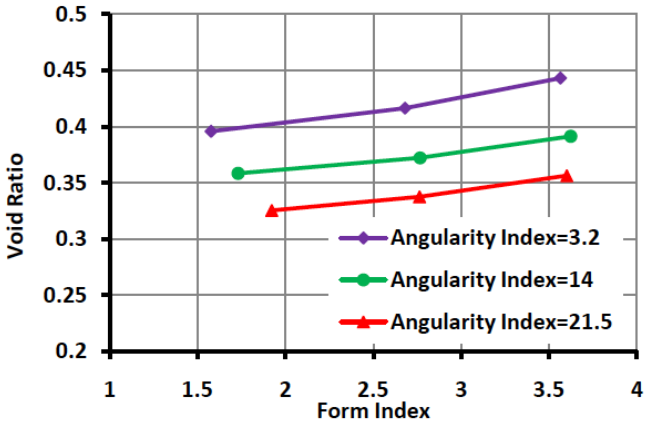

Figure 6: Relationship between form index and angularity index with void ratio.

4. SIZE DISTRIBUTION OF BROKEN SANDSTONE

To investigate the behavior of broken rock, for each specimen, the size distribution of particles should be addressed as an important parameter. To determine the particles size distribution by using image processing method, the equivalent diameter of particle was calculated. The particle equivalent diameter is the diameter of a circle that has the same area with the particle. The determined particle size distribution through image processing results in bigger particle size compared with the sieve method. In a size distribution sieve analysis, particles may be oriented such that they do not pass a given size sieve-opening. An image processing method could hence yield a different size distribution. Figure **7** illustrates an ellipsoid particle oriented such that it may not pass a given size sieve opening. Particle size distributions via image processing techniques may then require a correction coefficient to be comparable to a more practical geotechnical particle size distribution sieve analysis. Califice [37] also confirmed that the particle geometry may affect size distribution determined via image analysis. Janaka [38] proposed a 0.86 correction coefficient to convert image processing results to an equivalent particle size distribution via a sieve approach.

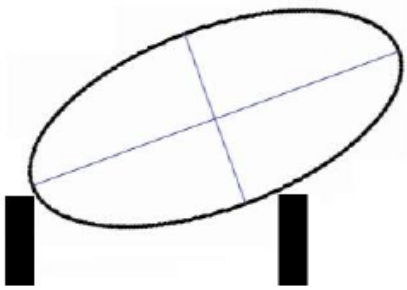

Figure 7: Particle not passing a sieve opening due to orientation.

The effect of particle shape on size distribution correction coefficient was investigated, where specimens of different form index were evaluated via both image processing and sieving methods. Results showed that the correction factor depends greatly on form index. It was shown that ellipsoid particles require smaller correction factors than those of more circular shape, as effectively an ellipsoid particle appears larger than a circular particle. The effect of particle shape on correction coefficient has a limitation; where those with a form index smaller than 1.6 suggest a correction

coefficient closer to 1, while an increasing circular nature of a particle with decreasing form index does not in fact affect the correction coefficient. Correction coefficients approaching 0.8 were shown to be appropriate for specimens with form indices larger than 2.4; where increasing ellipticity of a particle does not affect the correction coefficient further. Figure **8** shows the applied correction coefficient (F_{corr}) function to convert image processing to equivalent sieve size distributions based on specimen form index.

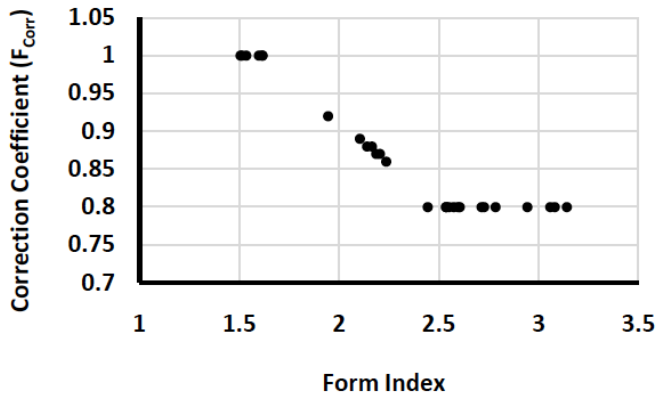

Figure 8: Relationship between correction coefficient (F_{corr}) and form index of specimen.

It was concluded here that correction coefficients between 1 and 0.8, as a function of form index, effectively convert image processing size distributions to equivalent sieve size distributions. Figure **9** illustrates particle size distributions determined using the image processing method and a sieve method for a sample with an average form index of 2.7, such that the correction factor was seen to be 0.8. Table **3** is a summary of the specimen particles size distribution parameters and corresponding correction coefficients (F_{corr}).

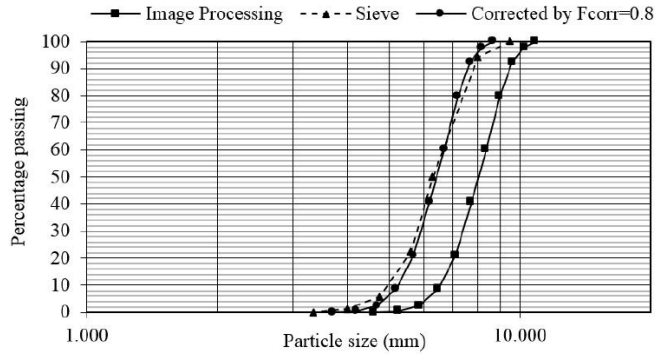

Figure 9: Size distribution comparison of particles with form index 2.7.

Table 3: A Summary of the Specimen Particles Size Distribution Parameters

Specimen No.	D_{60}	D_{50}	D_{10}	F_{corr}
S 1	8.6	8.4	6.8	1.00
S 2	7.5	7.3	5.9	0.80
S 3	7.0	6.8	5.4	0.88
S 4	9.2	8.8	7.0	0.80
S 5	7.6	7.5	6.0	0.80
S 6	8.7	8.3	6.1	0.87
S 7	7.9	7.6	6.0	0.80
S 8	7.8	7.5	5.9	0.80
S 9	8.5	8.3	7.0	1.00
S 10	9.1	8.8	7.1	0.80
S 11	7.6	7.1	5.7	0.87
S 12	7.0	6.6	5.2	0.80
S 13	8.8	8.4	6.4	0.80
S 14	8.5	8.2	6.7	1.00
S 15	7.2	6.8	5.4	0.80
S 16	6.5	6.2	5.1	0.86
S 17	9.0	8.4	6.0	0.80
S 18	7.9	7.7	6.2	1.00
S 19	6.7	6.4	5.4	0.80
S 20	6.7	6.4	5.0	0.89
S 21	5.9	5.4	1.1	0.80
S 22	6.9	6.0	1.8	1.00
S 23	6.7	6.5	5.3	0.80
S 24	8.1	7.8	6.3	1.00
S 25	6.6	6.3	5.1	0.88
S 26	5.6	4.9	0.9	0.92
S 27	5.2	4.4	0.9	0.80

5. TRIAXIAL TESTS ON BROKEN SANDSTONE

Given the low confining pressure needed for broken rock triaxial testing, a soil triaxial cell was adapted as the mode of load application. To prepare triaxial test specimens, broken Berea homogeneous fine-grained sandstone particles were again generated by a rock jaw crusher with a gape of 1 cm. The physical and mechanical properties of the intact sandstone are summarized in Table **4**.

The following procedure was used for sample preparation prior to triaxial tests: Crush sandstone using a rock jaw crusher with 1 cm gap; sieve the crushed rock to remove particles < 6 mm and > 12 mm;

determine the shape characteristics of particles via image analysis; fill a soil neoprene sleeve membrane with broken rock using a cylindrical mould; vibrate the specimen and membrane at 60 Hz to reconfigure and compact the broken rock.

Table 4: Summary of the Physical Properties of Sandstone

Parameter	Value
Density	2300 kg/m^3
Young Modulus	1950 MPa
Uniaxial strength of Intact Rock	32 MPa
Internal Friction Angle of Intact Rock	44°
Hock Parameter (m_i)	11

In conducting the triaxial tests, some broken rock specimens failed prematurely due to the rubber membrane being punctured by sharp particles or due to eccentric deformation of the specimen. When the membrane was found to have been punctured by a particle, water flowed into the specimen decreasing frictional strength evident via the: confining pressure suddenly decreasing; air bubbles appearing around a specimen during a test; visual appearance of water inside the membrane; or water evident within the membrane after a test.

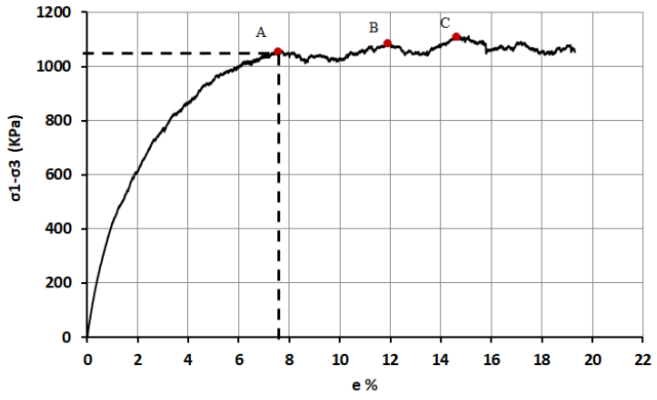

Figure 10: Triaxial stress-strain plot for broken Berea sandstone at 276 kPa confining pressure.

Determining peak axial strength for broken rock specimens from axial stress-strain plots proved somewhat difficult as several points could be considered as peak values. Figure **10** shows an example axial stress-strain plot. Three points could be considered as a possible peak strength indicator. Here, the first maximum point (point A) was taken as the peak strength. It was thus assumed that after the first maximum point (point A), breakage of some particles could potentially occur, changing the relative particle orientations within a specimen.

As attested to by other research in this area, the results of the triaxial tests indicated that confining pressure and void ratio of broken rock have a significant impact on strength. In addition, particle geometry and relative orientation generated an appreciable impact on the behavior of broken rock. Given that frictional behavior between particles dominated behavior at low confining pressure, the strength of broken rock and the confining pressure were expected to be directly proportional. Figure **11** illustrates a suggested power relationship to the triaxial test results, therein suggesting that a power relationship between minor and major principal stress is a reasonable descriptor of the behavior of broken rock.

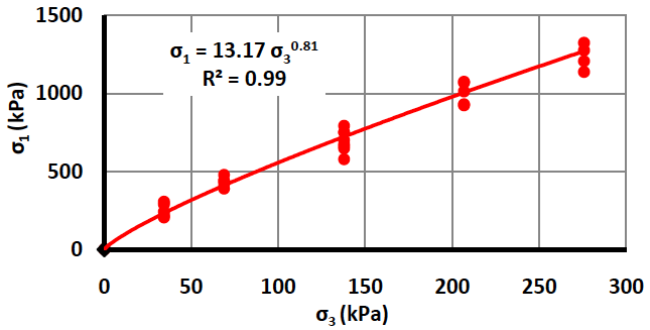

Figure 11: A power function estimating the strength of broken Berea sandstone.

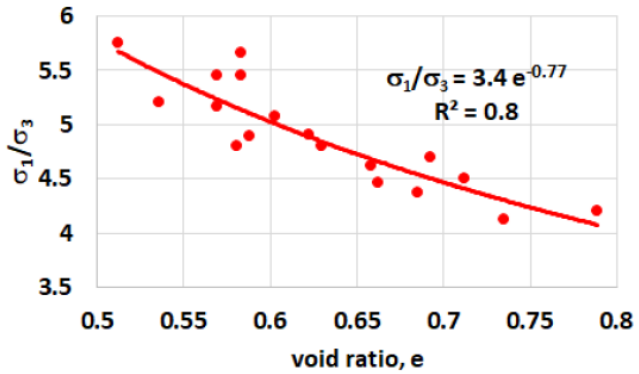

Figure 12: Void ratio versus strength for broken Berea sandstone.

Figure **12** illustrates the relationship between void ratio and applied stress ratio. It is clear that void ratio and specimen strength are inversely related for any given confining pressure. Equation 8 may be used to model broken rock strength, as a function of void ratio and applied confining pressure.

$$\sigma_1 = 3.4\ \sigma_3\ e^{-0.77} \quad (8)$$

Figure **13** shows a discerned relationship from the triaxial tests for the ratio of form index (FI) to angularity index (AI) as a function of the applied stress ratio, σ_1/σ_3. This suggests that broken rock comprising higher angular particles (higher angularity index) and isodiametric particles (lower form index) exhibit higher strength, which should not be a surprise. Broken rock with isodiametric particles has a lower void ratio and higher strength. Furthermore, broken rock with higher angular particles have lower void ratio and higher strength. Broken rock with higher angular and isodiametric particles has lower FI/AI, lower void ratio, resulting in higher strength.

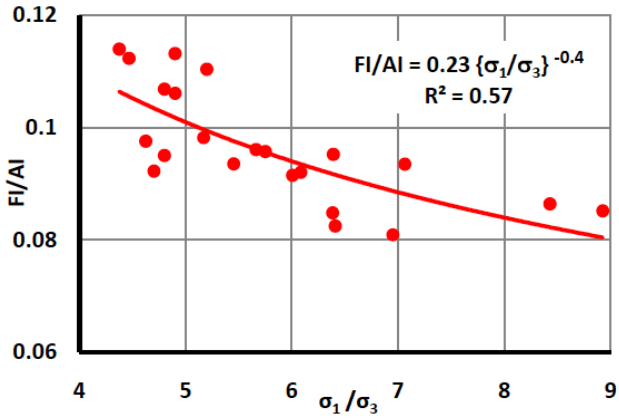

Figure 13: Suggested trend between form/angularity and applied stress ratios.

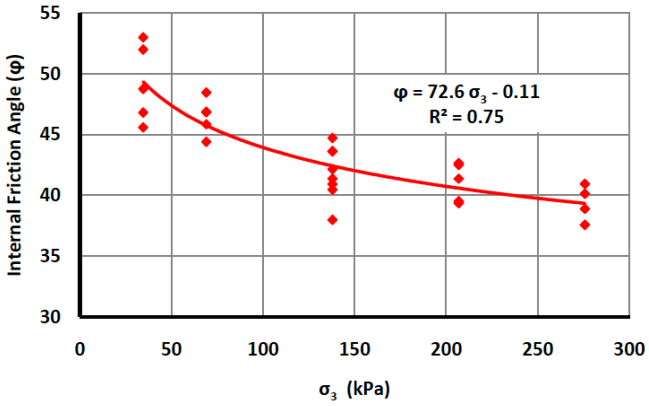

Figure 14: Relationship between peak internal friction angle and confining pressure.

Internal friction angle and confining pressure were shown to be inversely related; where an increase in confining pressure decreases the effective internal friction angle of broken rock, Figure **14**.

CONCLUSIONS

Form, angularity and texture are three independent parameters that describe particle geometry. Particle geometry was determined in this paper via an image processing method adapting previously identified formulae. Form index, form factor, angularity index, angularity parameter and texture parameter were investigated for broken Berea sandstone. Results established during the course of this paper may be summarized as: The geometry of crushed sandstone yielded form index and angularity index a better indicator of particle geometric characteristic for the crushed Berea sandstone.

Triaxial strength tests were conducted on specimens of broken Berea sandstone rock at varying confining pressure. The results were analyzed relative to particle shape characteristics; showing that confining pressure and void ratio have a significant impact on the strength of broken rock, where particle shape characteristics impact specifically the frictional (strength) resistance. Particle geometry affects the resistance of particles to move relative to each other, via sliding resistance between particles, a function of void ratio and the number of contact points between particles.

- Increasing the confining pressure enhances the strength of broken rock.
- Void ratio and broken rock strength are inversely related.
- The internal friction angle and confining pressure are inversely related for broken rock.
- Form index is directly proportional to void ratio, with decreasing broken rock strength.
- Angularity index is inversely proportional to void ratio. Increasing angularity index increases broken rock strength.

REFERENCES

[1] Feda J. Mechanics of Particulate Materials. New York: Elsevier Science Publishing Company; 1982. https://www.elsevier.com/books/mechanics-of-particulate-materials/feda/978-0-444-99713-5

[2] Marsal Rj. Frictional Resistance of Granular Soils. Seventh International Conference on Soil Mechanics and Foundation Engineering; Mexico; 1969. https://www.tib.eu/en/search/id/-TIBKAT%3A349216401/Proceedings-of-the-seventh-International-Conference/

[3] Marsal Rj. Mechanical Properties of Rockfill. Embankment Dam Engineering. 1973: 12. https://www.library.ualberta.ca/-catalog/567869

[4] Mogami T, editor On the Angle of Internal Friction of Rockfill Materials. Contributions and Discussions on Mechanical Properties of Rockfill and Gravel Materials; 1969: Mexico

[5] Fumagalli E. Tests on Cohesionless Materials for Rockfill Dams. Journal of Soil Mechanics & Foundations Div. 1969; 95(1): 313-30. http://cedb.asce.org/CEDBsearch/-record.jsp?dockey=0016209

[6] Hobbs DW. A study of the behaviour of a broken rock under triaxial compression, and its application to mine roadways. Int J Rock Mech Min Sci. 1966; 3: 33. https://www.sciencedirect.com/science/article/pii/0148906266900301
https://doi.org/10.1016/0148-9062(66)90030-1

[7] Hobbs DW. The behavior of broken rock under triaxial compression. Int J Rock Mech Min Sc. 1970; 7: 23. https://www.sciencedirect.com/science/article/pii/0148906270900082

[8] Hussaini MA. Influence of end restraint and method of consolidation on the drained triaxial compressive strength of crushed Napa basalt. Vicksburg: Waterways Experiment Station; 1970. http://classify.oclc.org/classify2/-ClassifyDemo?owi=14954414

[9] Hussaini MA. Plane strain and triaxial compression tests on crushed napa basalt. Vicksburg: Waterways Experiment Station; 1971. http://classify.oclc.org/classify2/ClassifyDemo?owi=1862915613

[10] Hussaini MA. Effect of particle size and strain conditions on the strength of crushed basalt. Canadian Geotechnical Journal. 1983; 20(4): 12. http://www.nrcresearchpress.com/-doi/abs/10.1139/t83-077#.W-OYE9VKjIU

[11] Joseph TG. Estimation of the post-failure stiffness of rock. Edmonton, Canada: University of Alberta; 2000. https://www.library.ualberta.ca/catalog/2511375

[12] Joseph TG, Barron K. The post-failure characteristics of rock. CIM Bulletin. 2003; 96, N° 1070:9. https://store.cim.org/en/-the-post-failure-characteristics-of-rock

[13] Barrett PJ. The shape of rock particles, a critical review. Sedimentology. 1980; 27: 291-303. https://onlinelibrary.wiley.com/doi/abs/10.1111/j.1365-3091.1980.tb01179.x
https://doi.org/10.1111/j.1365-3091.1980.tb01179.x

[14] Masad E. Review Of Imaging Techniques For Characterizing The Shape of Aggregates Used in Asphalt Mixes. International Center for Aggregates Research 9th Annual Symposium: Aggregates - Concrete, Bases and Fines; Austin, Texas; 2001. https://trid.trb.org/view.aspx?id=746676

[15] Masad E. The Development of a Computer Controlled Image Analysis System for Measuring Aggregate Shape Properties. Washington, D.C: National Cooperative Highway Research Program NCHRP-IDEA Project 77, Transportation Research Board, National Research Council; 2003; Report No.: Final Report.
http://onlinepubs.trb.org/onlinepubs/archive/studies/idea/finalreports/highway/NCHRP077_Final_Report.pdf

[16] Masad E, Al-Rousan T, Button J, Little D, Tutumluer E. Test Methods for Characterizing Aggregate Shape, Texture, and Angularity. WASHINGTON, D.C.: National Cooperative Highway Research Program; 2007; Report No.: NCHRP Report 555. http://www.trb.org/main/blurbs/158468.aspx

[17] Little D, Button J, Jayawickrama P, Solaimanian M, Hudson B. Quantify Shape, Angularity and Surface Texture of Aggregates Using Image Analysis and Study Their Effect on Performance. Texas: Texas Transportation Institute, The Texas A&M University System, College Station; 2003. https://trid.trb.org/view/778725

[18] Al-Rousan TM. Characterization of Aggregate Shape Properties Using a Computer Automated System College Station: Texas A&M University; 2004. https://oaktrust.library.tamu.edu/handle/1969.1/1485

[19] Al-Rousan TM, Masad E, Tutumluer E, Pan T. Evaluation of Image Analysis Techniques for Quantifying Aggregate Shape Characteristics. Construction and Building Materials. 2007; 21: 978-90. https://www.sciencedirect.com/science/article/-abs/pii/S0950061806000377
https://doi.org/10.1016/j.conbuildmat.2006.03.005

[20] Azevedo NM, Lemos JV. Aggregate shape influence on the fracture behaviour of concrete. Structural Engineering and Mechanics, An Int'l Journal 2006; 24(4). https://www.edemsimulation.com/papers/aggregate-shape-influence-on-the-fracture-behaviour-of-concrete/

[21] Zhou L, Chu X, Zhang X, Xu Y. Numerical investigations on breakage behaviour of granular materials under triaxial stresses. Geomechanics and Engineering, An Int'l Journal. 2016; 11(5):639-55. http://www.techno-press.org/content/-?page=article&journal=gae&volume=11&num=5&ordernum=3

[22] Afshar T, Disfani MM, Arulrajah A, Narsilio GA, Emamc S. Impact of particle shape on breakage of recycled construction and demolition aggregates. Powder Technology. 2017; 308. https://www.sciencedirect.com/science/-article/pii/S003259101630835X
https://doi.org/10.1016/j.powtec.2016.11.043

[23] Chen C, An X. Model for simulating the effects of particle size distribution on the hydration process of cement. Computers and Concrete, An Int'l Journal 2012; 9(3). http://www.techno-press.org/content/?page=article&journal=cac&volume=9&num=3&ordernum=2

[24] Masad E, Olcott D, White T, Tashman L. Correlation of Fine Aggregate Imaging Shape Indices with Asphalt Mixture Performance. Washington, D.C: Transportation Research Record 1757. Transportation Research Board, National Research Council; 2001. https://trrjournalonline.trb.org/-doi/abs/10.3141/1757-17?journalCode=trr

[25] Wang LB, Park JY, Mohammad LN. Quantification of Morphology Characteristics of Aggregate From Profile Images. 82nd Transportation Research Board Annual Meeting; Washington, D.C. 2003; p. 23. http://classify.oclc.org/classify2/ClassifyDemo?wi=51462777

[26] Arasan S, Hasiloglu AS, Akbulut S. Shape Properties of Natural and Crushed Aggregate using Image Analysis. International Journal of Civil and Structural Engineering. 2010; Volume 1, No 2: 221-33. http://www.ipublishing.co.in/-jcandsevol1no12010/EIJCSE1018.pdf

[27] Masad EA, Little DN, Tashman L, Saadeh S, Al-Rousan T, Sukhwani R. Evaluation of Aggregate Characteristics Affecting HMA Concrete Performance. Texas: Texas Transportation Institute; 2003. https://repositories.lib.utexas.edu/handle/2152/35367

[28] Kuo C-Y, Freeman RB. Imaging Indices for Quantification of Shape, Angularity, and Surface Texture of Aggregates. Transportation Research Record: Journal of the Transportation Research Board. 2000; 1721: 57-65. https://trrjournalonline.trb.org/doi/abs/10.3141/1721-07

[29] Tutumluer E, Rao C, Stefanski JA. Video Image Analysis of Aggregates. Urbana, IL: University of Illinois Urbana-Champaign; 2000. Report No.: FHWA-IL-UI Contract No.: 278. https://www.ideals.illinois.edu/handle/2142/46350

[30] Fletcher T, Chandan C, Masad E, Sivakumar K. Aggregate Imaging System (AIMS) for Characterizing the Shape of Fine and Coarse Aggregates. 82nd Transportation Research Board Annual Meeting; Washington, D.C.2003. p. 31. http://classify.oclc.org/classify2/ClassifyDemo?wi=51462777

[31] Swift GA. Characterization of Coarse Aggregate Angularity Using Digital Image Processing. Columbia, USA: University of Missouri; 2007. https://scholarsmine.mst.edu/-cgi/viewcontent.cgi?article=5579&context=masters_theses

[32] Wang L, Lane DS, Lu Y, Druta C. Portable Image Analysis

System for Characterizing Aggregate Morphology. Journal of the Transportation Research Board. 2009; 3-11. https://vtechworks.lib.vt.edu/handle/10919/46643 https://doi.org/10.3141/2104-01

[33] Koohmishi M, Palassi M. Evaluation of morphological properties of railway ballast particles by image processing method. Transportation Geotechnics. 2017; 12. https://www.sciencedirect.com/science/article/pii/S2214391217301104

[34] Gray WA. The Packing of Solid Particles. London: Chapman & Hall; 1968. http://www.worldcat.org/title/packing-of-solid-particles/oclc/596402826

[35] Donev A, Connelly R, Stillinger FH, Torquato S. Hypoconstrained Jammed Packings of Nonspherical Hard Particles: Ellipses and Ellipsoids. Phys Rev E. 2007; 75(5): 35. https://arxiv.org/ftp/cond-mat/papers/0608/0608334.pdf https://doi.org/10.1103/PhysRevE.75.051304

[36] Delaney GW, Cleary PW. The packing properties of superellipsoids. EPL (Europhysics Letters). 2010; 89(3). http://iopscience.iop.org/article/10.1209/0295-5075/89/34002/meta https://doi.org/10.1209/0295-5075/89/34002

[37] Califice A, Michel F, Dislaire G, Pirard E. Influence of particle shape on size distribution measurements by 3D and 2D image analyses and laser diffraction. Powder Technology. 2013; 237. ttps://www.sciencedirect.com/-science/article/pii/S003259101300020X

[38] Janaka GHA, Kumara J, Hayano K, Ogiwara K. Image Analysis Techniques on Evaluation of Particle Size Distribution of Gravel. Int J of GEOMATE. 2012; 3(1): 290-7. http://www.geomatejournal.com/sites/default/files/articles/290-295-1261-kumara-sept-2012.pdf

Received on 9-11-2018 Accepted on 29-12-2018 Published on 30-12-2018

DOI: http://dx.doi.org/10.15377/2409-5710.2018.05.3